

Class-Independent Increment: An Efficient Approach for Multi-label Class-Incremental Learning

Songlin Dong, Yuhang He, Zhengdong Zhou, Haoyu Luo, Xing Wei,
Alex C. Kot, *Fellow, IEEE*, Yihong Gong, *Fellow, IEEE*,

Abstract—Current research on class-incremental learning primarily focuses on single-label classification tasks. However, real-world applications often involve multi-label scenarios, such as image retrieval and medical imaging. Therefore, this paper focuses on the challenging yet practical multi-label class-incremental learning (MLCIL) problem. In addition to the challenge of catastrophic forgetting, MLCIL encounters issues related to feature confusion, encompassing inter-session and intra-feature confusion. To address these problems, we propose a novel MLCIL approach called class-independent increment (CLIN). Specifically, in contrast to existing methods that extract image-level features, we propose a class-independent incremental network (CINet) to extract multiple class-level embeddings for multi-label samples. It learns and preserves the knowledge of different classes by constructing class-specific tokens. On this basis, we develop two novel loss functions, optimizing the learning of class-specific tokens and class-level embeddings, respectively. These losses aim to distinguish between new and old classes, further alleviating the problem of feature confusion. Extensive experiments on MSCOCO and PASCAL VOC datasets demonstrate the effectiveness of our method for improving recognition performance and mitigating forgetting on various MLCIL tasks.

Index Terms—Multi-label class-incremental learning, Feature confusion, CINet, Class-level embedding, Contrastive loss.

I. INTRODUCTION

In the past decade, deep learning has catalyzed significant breakthroughs in computer vision and multimedia tasks, including image classification [1], [2], semantic segmentation [3], and object detection [4], [5], among others. However, the deep learning-based methods fail to recognize new samples of unseen classes. Directly learning these new samples will lead to *catastrophic forgetting* (CF), where the model’s performance on historical data significantly deteriorates. In this case, class-incremental learning (CIL) [6]–[10] is extensively studied to update the model only with new class data in each task while preserving the knowledge of old classes. However, in practical applications, an image typically contains multiple objects. For example, photos on social media often contain multiple labels or objects, making traditional CIL methods that assume each image contains only one object unsuitable. Therefore, some work explores studying CIL in the multi-label scenario, named

Songlin Dong, Haoyu Luo, and Yuhang He are with the College of Artificial Intelligence, Xi’an Jiaotong University; Zhengdong Zhou, Xing Wei, and Yihong Gong are with the College of Software Engineering, Xi’an Jiaotong University. Alex C. Kot is with the School of Electrical and Electronic Engineering at Nanyang Technological University. (e-mail: {dsl972731417, luohaoyu, 3123358165}@stu.xjtu.edu.cn; heyuhang@xjtu.edu.cn; eackot@ntu.edu.sg; {weixing, ygong}@mail.xjtu.edu.cn).

Yuhang He is the corresponding author.

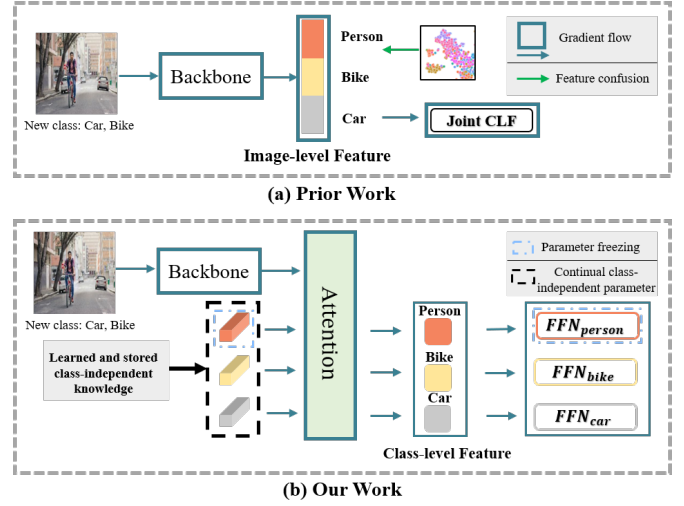


Fig. 1: Comparison between **prior work** and **our work** (a) The prior paradigm for MLCIL. Prior methods employ image-level (task-level) features and train a joint classifier for each session. (b) Our proposed paradigm. We employ a CLIN framework to generate and process class-level features to solve the feature confusion problem. Moreover, we design two loss functions to prevent confusion between old and new classes.

multi-label class-incremental learning (MLCIL) [11]–[14]. It aims to gradually learn new classes from label-incomplete multi-label data streams in different learning stages while maintaining performance on old labels.

Compared to the traditional (*i.e.* single-label) CIL problem, it is more challenging as a single image may contain multiple objects of both the old and new classes, with only new class objects (one or multiple categories) annotated in each learning session. To this end, prior methods to address forgetting for MLCIL tasks include exemplar replay (ER), knowledge distillation (KD), and network expansion (NE). ER-based methods [13], [14] solve the CF problem by storing a small number of old class exemplars. They replay the exemplars with the current session samples to mitigate the old class forgetting when learning new classes. KD-based methods [11], [15], [16] design regularization terms on the image-level feature to preserve previous knowledge when training the model on new data. The NE-based approaches [11], [17] allocate a distinct set of parameters (e.g., tokens, prompts) for each session to learn task-level features. During the training process, parameters associated with old classes irrelevant to the current session are frozen to prevent forgetting old class knowledge.

Despite their promising progress, these existing methods suffer from the *feature confusion* problem, which hampers their performance in knowledge learning and maintenance, especially when a single image contains both old and new class objects. The *feature confusion* is two-fold, *i.e.*, the inter-session confusion and intra-feature confusion. Firstly, during the incremental learning process, as the categories of different sessions are disjoint and trained separately, it is difficult to establish sharp decision boundaries between old and new classes, resulting in feature confusion between new and old classes, known as the *inter-session confusion* [18] problem. This problem is more pronounced in multi-label tasks with multiple targets in a single, leading to a significant performance decline in MLCIL. Secondly, as shown in Fig. 1 (a), all existing methods extract an image-level feature for an image during the incremental learning process. However, as a single image may contain multiple classes in MLCIL, the image-level feature will lead to intra-feature confusion during the incremental learning process. For example, in Fig. 1 (a), the image contains a **man** riding his **bike** behind a **car**. Extracting an image-level feature for this image will not only mix the features of these three classes but also lead to label conflict [11] as the classes are learned in different incremental sessions, resulting in class confusion and semantic conflict within the image-level feature, *i.e.*, the *intra-feature confusion problem*.

To bridge this gap, we propose a novel framework for MLCIL, named **CL**ass-Independent **IN**crement (CLIN). Different from the existing methods that extract an image-level feature for MLCIL, we propose a novel class-independent incremental network (CINet) to extract multiple class-level embeddings for input images containing multiple classes and learn and maintain the knowledge of different classes by constructing class-specific tokens as shown in Fig. 1 (b). The CINet comprises a *class-level cross-attention* module and a *class-independent classifier*. The former module takes class-specific tokens as input, where each token corresponds to a specific class. It leverages attention mechanisms to extract and generate class-level embeddings associated with each class, effectively producing class-level features and thereby transforming the multi-label problem into multiple single-label problems. Moreover, it can effectively extract local discriminative features and explore correlations between labels as a special Transformer decoder [19]–[21]. Subsequently, the class-independent classifier replaces the previous joint classifier, establishing a one-to-one correspondence between class-level embeddings and class labels. It predicts the presence of the corresponding labels through binary classification, reducing interference in learning between new and old classes. During incremental learning, we dynamically extend the class-specific tokens and the class-independent classifier to acquire new knowledge and freeze the tokens and classification heads associated with old classes to prevent forgetting. The proposed CINet not only effectively generates and processes class-level features to address the feature confusion problems but also alleviates inter-session confusion by maintaining knowledge for each old class through a small number of parameters independent of the shared model.

On this basis, to further address the feature confusion

problem in MLCIL, we introduce two novel loss functions to optimize the learning of class-specific tokens and class-level embeddings, respectively. Concretely, we address the challenge of applying metric learning to multi-label tasks and propose a contrastive loss on class-level embeddings, *i.e.* *multi-label contrastive loss*, aimed at minimizing intra-class distances and maximizing inter-class distances. Moreover, we introduce a *token orthogonal loss* on the task-specific tokens to alleviate the conflict between old knowledge maintenance and new knowledge learning. Our model achieves significant performance improvements on both existing MLCIL protocols [11], [12]. Moreover, our method maintains high performance in a rehearsal-free setting, significantly saving storage space.

The key contributions of this paper are summarized as follows:

- We propose a novel and effective method, CLIN, which utilizes class-level rather than image-level features to address the MLCIL task. Our approach effectively addresses the feature confusion problem and achieves notable performance improvements.
- We design a novel scalable network, CINet, consisting of a class-level cross-attention module and a class-independent classifier for class-level embedding generation and class-specific knowledge retention.
- We propose a multi-label contrastive loss and introduce a token orthogonal loss to mitigate the interaction between old and new knowledge.
- We conducted extensive experiments on two well-established protocols, achieving improvements of up to **4.3%** and **8.4%**, respectively. Furthermore, we evaluated our method in a rehearsal-free setting, achieving state-of-the-art performance and highlighting its robustness.

II. RELATED WORK

A. Single-Label Incremental Learning

Mainstream single-label incremental learning research can be broadly divided into the following four categories:

Rehearsal-based methods maintain a set of exemplars representing existing data for simultaneous training with new data from the current task. These methods primarily address the challenge of CIL [6], [22]–[24] problem. For instance, ER [25] establishes a memory buffer to store samples from previous tasks for retraining with new data, while DER++ [24] suggests applying knowledge distillation penalties to the stored data. Moreover, iCaRL [6] and its variations [9], [22], [23], [26], [27] prevent forgetting by utilizing the herding technique to select exemplars and formulate distinct KD losses. BIC [28] and other methods [29], [30] incorporate an additional bias correction process to adapt the classification layer. Recent approaches [31]–[33] introduce adaptive aggregation networks or emulate the feature space distribution of Oracle to enhance rehearsal-based methods.

Regularization-based methods incorporate a regularization term into the loss function to preserve prior knowledge in updated parameters. 1) Parameter regularization involves minimizing the variance of parameters associated with previous tasks [34]–[36]. For instance, EWC [34] utilizes a Fisher matrix

to protect crucial parameters from past tasks. Subsequently, oEWC [36] and other techniques [35], [37] continuously refine the calculation of parameter significance. 2) Data regularization consolidates previous knowledge by leveraging earlier models as soft teachers [38], [39]. LWF [38], for example, employs knowledge distillation to mitigate forgetting.

Architectural-based methods provide distinct parameters for each task to prevent forgetting. For example, Abati et al. [40], [41] and Rusu et al. [42] have proposed various strategies to isolate old and new task parameters, including duplicating a new network for each task to transfer previous knowledge through lateral connections. Recent architectural approaches [43], [44] combined with the rehearsal methods achieve a better anti-forgetting effect. These methods dynamically expand or prune the network parameters to accommodate the new data at the expense of limited scalability.

Prompt-based methods learn a small set of insertable pre-trained model prompts instead of directly modifying the encoder parameters. For example, L2P [7] creates only a pool of prompts inserted into the model and matches input images to prompts with image-wise prompt queries. DualPrompt [17] proposes multiple pools of prompts, including G-Prompts and E-Prompts for learning task-invariant and task-specific knowledge. Moreover, S-Prompts [45] learns the prompts domain by domain and incrementally inserts the learned prompts into a pool designed for domain-incremental learning. This setting involves learning the same set of classes under covariate distribution task shifts. It is distinct from the CIL setting presented in our paper, where the goal is to learn emerging object classes in new sessions.

B. Other Incremental Learning

Incremental Object Detection (IOD) focuses on applying incremental learning techniques specifically to object detection. Both knowledge distillation (KD) and experience replay (ER) have found applications in IOD tasks across different detectors. The work by [46] pioneers the use of KD on the output of Faster R-CNN, and subsequent methods [47], [48] extend this by adding KD terms on intermediate feature maps and region proposal networks or by maintaining a set of exemplars for fine-tuning the model. In addition to being implemented on CNN detectors, ER and KD techniques have also been employed in the transformer network DETR [49].

Incremental Semantic Segmentation (ISS) methods can be categorized into regularization-based and replay-based approaches. The former, exemplified by methods like SDR [50] and PLOP [51], introduce various KD strategies to regularize a current model within a latent feature space. The latter approaches [52], [53] rely on an ER strategy involving the retention of a small set of exemplars or pseudo information for previous categories.

Methods developed for incremental object detection (IOD) and incremental semantic segmentation (ISS) cannot be directly applied to MLCIL tasks, as they rely on specific detection and segmentation frameworks or require pixel-level and additional bounding box information. Therefore, research focusing on MLCIL with only image-level annotations holds significant value and importance.

C. Multi-label Classification

Multi-label classification (MLC) aims to gain a comprehensive understanding of objects and concepts in an image and the proposed methods can be categorized into two main directions:

Label dependencies: Due to the multi-label nature of the data, the co-occurrence relationships between labels can be mined as prior knowledge. [54] first proposes a ranking-based learning strategy to train CNN for multi-label classification. [55] and [56] exploit label dependencies by utilizing recurrent neural networks (RNNs) and long short-term memory (LSTM). Moreover, the GCN is also proven to be more effective in modeling label dependencies [2], [57], [58]. Recently, Transformers have also been developed for multi-label classification tasks and have shown great potential [19]–[21]. [20] leverages Transformers to exploit the complex dependencies among visual features and labels. [19] leverages Transformer decoders to adaptively extract local discriminative features for different classes and query the existence of a class object.

Loss functions: The primary challenge in MLC is the significant imbalance between positive and negative instances. To address this, [59] suggests a distribution-balanced loss to reduce imbalance. Another common solution is focal loss [60], which pays more attention to hard samples while less to easy samples. The recent method [61] proposes a novel asymmetric loss, which applies the dynamic down-weight and the hard threshold to easy negative samples while discarding possibly mislabeled samples.

Some MLC methods [19]–[21] utilize Transformer decoders to query the existence of class labels, establishing a relationship between queries and labels. However, these methods establish the relationship only once in a supervised learning setting, lacking scalability. These methods face severe catastrophic forgetting in MLCIL, as observed in experiments like FT.

D. Multi-Label Stream Learning.

Multi-label stream learning (MSL) [62]–[66], also known as dynamic multi-label learning or new label emerging, involves reusing previously learned models and creating new classifiers for newly emerging labels. In instance data streams, aside from the initial training set, subsequent data does not have class labels available. Therefore, detecting and modeling new labels becomes the primary challenge. For example, MLF [62] assumes that new labels are linear combinations of other labels and inherits the relationships between labels through classifiers. MuENL [64] and [67] design detectors based on input features and predicted label attributes and propose algorithms for updating the classifier. DSDL [65] employs streaming label mapping to extract relationships between labels and uses knowledge distillation to transfer knowledge for modeling new labels. FSSL [68] generates label-specific features and effectively fuses these features for newly arrived labels. CIFDM [69] focuses on label correlation and feature embedding space to continuously learn how to predict new labels. ANT [70] trains a student by learning from each teacher’s partial knowledge of label dependencies to infer global dependencies across all labels.

MSL can be considered a special form of weakly supervised learning [64]. Since the data stream for new classes is unlabeled, the core focus is on detecting the emergence of new labels and modeling the relationships between new and known labels rather than on whether known labels are forgotten. This is fundamentally different from the MLCIL setting. MLCIL tasks require learning new classes without forgetting old ones and being able to perform MLC on all previously learned classes. Therefore, MSL approaches cannot be directly applied to MLCIL tasks.

E. Multi-Label Class Incremental Learning

Multi-label class incremental learning aims to continually construct a unified classifier that can constantly learn and integrate the knowledge and make a comprehensive understanding of class objects in an image. For example, AGCN and its variant [15], [16] employed an augmented Graph Convolutional Network to capture the co-occurrence correlation among classes and incrementally expanded the graph during the learning process. PRS [14] and OCDM [13] enhanced the sampling methods for online data streams, aiming to sample a buffer that is closer to the real distribution to mitigate the imbalance problem. However, these methods belong to online learning settings (i.e., each batch of data can only be accessed once) which exhibit suboptimal performance in offline settings [11].

Then, KRT [11] defines a more promising task: multi-label class-incremental learning and utilizes an extensible ICA module with token distillation loss to store and transfer knowledge, mitigating catastrophic forgetting. Moreover, APPLE [12] introduces a novel MLCIL benchmark protocol and presents a novel framework that addresses catastrophic forgetting in MLCIL tasks through an adaptive pseudo-label strategy, a cluster sampling method, and a class attention decoder. We build upon the foundation of this method and conduct comprehensive comparative experiments on two offline MLCIL protocols.

III. METHOD

A. Problem Formulation

The multi-label class-incremental learning problem [11], [12] is defined as follows: suppose we have T sequences of multi-label image sets $\{\mathbf{D}^1, \mathbf{D}^2, \dots, \mathbf{D}^T\}$, where $\mathbf{D}^t = \{\mathbf{X}^t, \mathbf{Z}^t\}$ is consisted of a training set \mathbf{X}^t and a test set \mathbf{Z}^t . Each training set is defined as $\mathbf{X}^t = \{(\mathbf{x}_i^t, \mathbf{y}_i^t)\}_{i=1}^{N^t}$, where N^t represents the number of training samples, \mathbf{x}_i^t is the i -th training sample and $\mathbf{y}_i^t \subseteq \mathbf{C}^t$ is a label set with $1 \leq |\mathbf{y}_i^t| \leq |\mathbf{C}^t|$. \mathbf{C}^t denotes the class collection at the t -th session and $\forall m, n (m \neq n)$, $\mathbf{C}^m \cap \mathbf{C}^n = \emptyset^1$. In the MLCIL setting, a *multi-label classification* model is required to incrementally learn a *unified* classifier from a sequence of training sessions. At session t , only \mathbf{X}^t is available during training and the model is evaluated on a combination of test sets $\mathbf{Z}^{1 \sim t} = \mathbf{Z}^1 \cup \dots \cup \mathbf{Z}^t$ and is expected to recognize *all* the encountered classes $\mathbf{C}^{1 \sim t} = \mathbf{C}^1 \cup \dots \cup \mathbf{C}^t$ present in the test images.

¹The training set images from different sessions can be repeated, but the annotated labels are different in [11], i.e., $X_m \cap X_n \neq \emptyset$. In protocol [12], image repetition is strictly restricted, i.e., $X_m \cap X_n = \emptyset$.

B. Overall Framework

Fig. 2 illustrates the pipeline of the CLIN approach. The structure of CLIN comprises two main components: a feature extractor backbone and a class-independent incremental network (CINet). The pre-trained feature extractor is represented by $f(\cdot; \theta)$, which is continual training during the incremental learning process. The class-independent incremental network comprises a class-level cross-attention module and independent classifiers. The former module is defined as $\gamma(\cdot; \omega)$, with a set of trainable class-specific tokens $\{\mathbf{q}_c\}_{c=1}^{|\mathbf{C}|}$, where $\mathbf{q}_c \in \mathbb{R}^D$, D denotes the dimension of token and $|\mathbf{C}|$ denotes the number of classes. The latter module is denoted as $\varphi(\cdot; \phi)$, including $|\mathbf{C}|$ mutually exclusive feed forward network (FFN) classifiers $\varphi(\cdot; \phi_c)$, where c denotes the class ID.

Assuming the t -th incremental session, the input of image x^t from \mathbf{D}^t is fed into the feature extractor $f(\cdot; \theta)$ and projected into the image token $X_P \in \mathbb{R}^{L \times D}$, where L is the token length and D is the feature dimension. Following this, X_P serves as input to the CINet and obtains class-level embeddings E^t . In the CINet, the $\gamma(\cdot; \omega)$ extends $|\mathbf{C}^t|$ (C_n) class-specific tokens (Orange one) to learn new classes and freeze $|\mathbf{C}^{1 \sim t-1}|$ (C_o) old tokens (Blue one) to prevent forgetting of old classes. To alleviate potential conflicts between the existing tokens and trainable tokens, we orthogonally initialize these tokens and maintain orthogonality through a token orthogonal loss \mathcal{L}_{to} .

Afterward, class-level embeddings E^t are mapped to a new space through a projection layer $\text{Proj}(\cdot)$, and in this projection space, a multi-label contrastive loss \mathcal{L}_{mc} is introduced to further improve the feature confusion problem. Moreover, similar to previous methods, to alleviate the forgetting of old knowledge, we design a knowledge distillation loss \mathcal{L}_{kd} on class-level embeddings E^t and old class-level embeddings E^{t-1} . Finally, the E^t is fed into the class-independent classifier $\varphi(\cdot; \phi)$ to perform the classification task and calculate \mathcal{L}_{ce} loss. Moreover, we follow the pseudo-labeling methods from previous works [11], [12] to mine old class information from input images. The following sections in this part will provide a detailed description of the CLIN method's structure and loss functions.

C. The Structure of Proposed CLIN

Unlike previous methods that leverage image-level representations for the MLCIL task, the CLIN approach proposes a novel class-independent incremental network to extract multiple class-level representations for each image and achieve incremental learning through network expansion and parameter freezing. The structure of CLIN consists of two main components: the feature extractor and class-independent incremental network as shown in Fig. 2.

Feature Extractor. Given an image $x \in \mathbb{R}^{H \times W \times 3}$ as input, we use a feature extractor to extract image-level features $f \in \mathbb{R}^{h \times w \times c}$, where h, w represent the height and width of the feature map, respectively, and c denotes the dimension of the features. Subsequently, we add a linear projection layer to project the features from dimension c to D to match with the dimension of the class-independent incremental network in the next stage and reshape the projected features to be patch tokens $X_p \in \mathbb{R}^{L \times D}$ where $L = hw$.

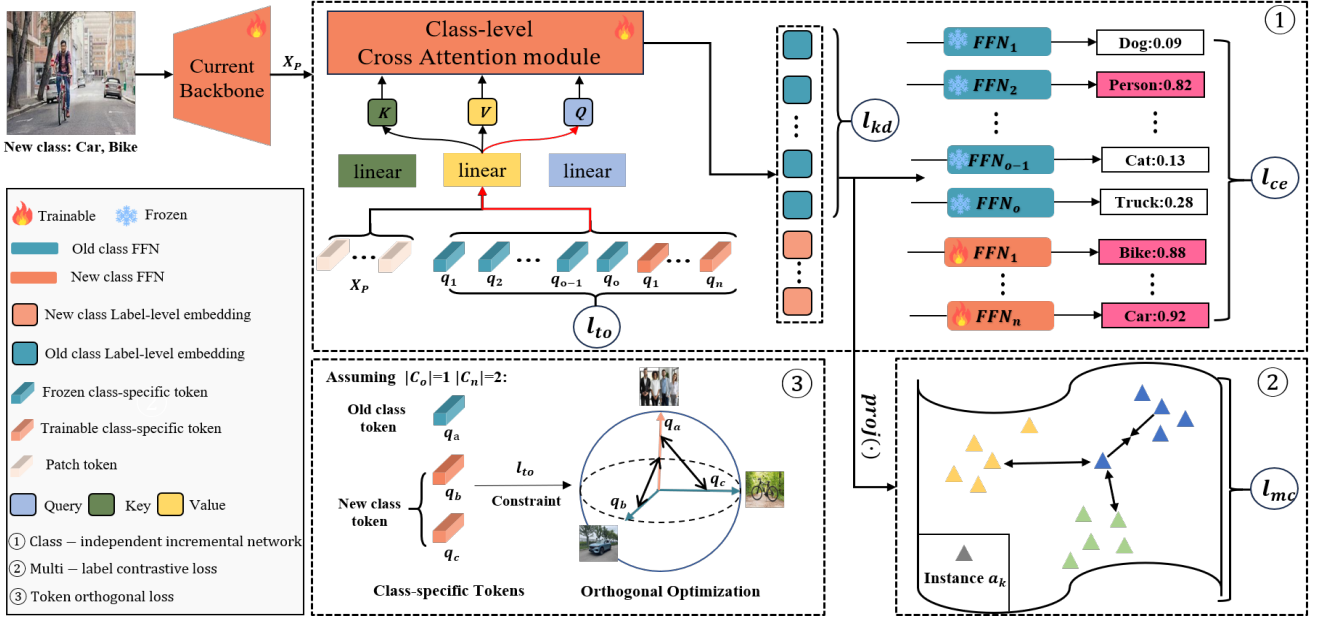


Fig. 2: The framework of proposed CLIN. During training, the image x^t (In actually, an input image can contain either one or multiple new classes, and it can also contain one, multiple, or no old classes.) undergoes feature extraction by the backbone and is then converted into patch tokens x_p . Together with a set of class-specific tokens, this forms the input for the class-level cross-attention module to generate class-level embeddings E^t . The set of class-specific tokens includes trainable tokens $\{q_c\}_{c=1}^{C_n}$ for new classes and frozen tokens $\{q_c\}_{c=1}^{C_o}$ for old classes, and compute \mathcal{L}_{to} to maintain orthogonality. Subsequently, E^t are separately fed into the class-independent classifier to compute \mathcal{L}_{ce} and a projection layer to calculate \mathcal{L}_{mc} .

Class-Independent Incremental Network. To implement and leverage class-level representations, we introduce the class-independent incremental network (CINet), consisting of two main components: a class-level cross-attention module with a set of trainable class-specific tokens and class-independent classifiers. In this chapter, we first introduce the fundamental structure of the CINet and subsequently elucidate how the CINet incrementally acquires new knowledge while preserving old knowledge in the MLCIL task.

(1) Class-level Cross-Attention: The first component of the CINet consists of a cross-attention module $\gamma(\cdot; \omega)$ and a set of learnable tokens $\{q_c\}_{c=1}^{|\mathcal{C}|}$, where $|\mathcal{C}|$ denotes the number of classes.

The first input to $\gamma(\cdot; \omega)$ is the patch tokens X_p obtained from the input image via a feature extractor. Moreover, to extract class-level representations and prevent confusion between new and old classes, we design a set of learnable tokens $\{q_c\}_{c=1}^{|\mathcal{C}|}$ (denoted as $X_q \in \mathbb{R}^{|\mathcal{C}| \times D}$), with the number of tokens matching the categories. Typically, the cross-attention module consists of two parts: multi-head attention block (MultiAttBlock) and multi-layer perceptron (MLP). It can be formalized as:

$$E_a = X_q + \text{MultiAttBlock}(\text{Norm}(X_q, X_p)), \quad (1)$$

$$E = E_a + \text{MLP}(\text{Norm}(E_a)), \quad (2)$$

Where $\text{MultiAttBlock}(\cdot)$ and $\text{Norm}(\cdot)$ denote the cross-attention and layer normalization in [71], respectively, and MLP is a multi-layer perceptron with a single hidden layer.

In the multi-head attention block, we use the class-specific token X_q as the Query (Q). Thus, through the multi-head self-

attention mechanism, the model can learn attention weights for specific embeddings of the labels. For example, if an image contains a **car**, the corresponding embedding is expected to be associated with a high attention weight for the **car** label. Meanwhile, the patch tokens X_p of the image serve as Key (K) and Value (V). Without loss of generality, it can be formulated as:

$$\begin{aligned} \mathbf{Q} &= \mathbf{W}_q X_q = \mathbf{W}_q [q_1, q_2, \dots, q_{|\mathcal{C}|}], \\ \mathbf{K} &= \mathbf{W}_k X_p, \\ \mathbf{V} &= \mathbf{W}_v X_p, \\ \mathbf{z} &= \mathbf{W}_o \text{softmax} \left(\frac{\mathbf{QK}^T}{\sqrt{l/h}} \right) \mathbf{V} + \mathbf{b}_o, \end{aligned} \quad (3)$$

where l is the embedding dimension, h is the number of attention heads.

As the key module of the CINet, the class-level cross-attention module takes an image-level feature as input and outputs its class-level representations, denoted by $E \in \mathbb{R}^{|\mathcal{C}| \times D}$. The class-level embeddings E keep the same dimension as class-specific tokens X_q (i.e. Query), where each row of E corresponds to the embedding of the image under the context of a specific class. Finally, class-level embeddings E are input into the class-independent classifier $\varphi(\cdot; \phi)$ for classification tasks.

(2) Class-independent Classifier: The input of the class-independent classifier is the class-level embeddings $E = \{e_1, e_2, \dots, e_{|\mathcal{C}|}\}$, where the class-level embedding e_c captures the features of the input image in the context of label c . To establish the correspondence between class labels and

class-level embeddings and to ensure no interference between different categories, especially between old and new classes, we utilize $|\mathbf{C}|$ separate Feed Forward Networks (FFNs) as classifiers instead of joint classifiers. It predicts the presence of corresponding labels through binary classification.

For each label c , FFN_c contains a linear layer and the parameters of $\varphi(\cdot; \phi_c)$ are a weight $w_c \in \mathbb{R}^{D \times 1}$ and a bias b_c . Specifically, we have a total of $|\mathbf{C}|$ independent FFNs as the classifier of $|\mathbf{C}|$ classes, which can be formulated as:

$$p_c = \sigma(w_c \times e_c + b_c), \quad c \in [1, |\mathbf{C}|] \quad (4)$$

where p_c is the prediction probability of c -th class, and σ is a sigmoid function.

(3) CINet Implements Incremental Learning. Assuming the t -th incremental session, the input image x^t with its class collection \mathbf{C}^t is initially processed through the feature extractor $f(\cdot; \theta)$ to obtain the patch tokens $X_p \in \mathbb{R}^{L \times D}$, serving as the image input component for the class-level cross-attention module.

As shown in Fig 2, we extend the class-specific token set by introducing vectors $X_q^t \in \mathbb{R}^{|\mathbf{C}^t| \times D}$, where the number of rows in the vectors corresponds to the number of new classes $|\mathbf{C}^t|$, i.e., each row vector represents a class-specific token to learn the knowledge of one new class. Additionally, the class-specific token set also includes already learned tokens for old classes $X_q^{1 \sim t-1} \in \mathbb{R}^{|\mathbf{C}^{1 \sim t-1}| \times D}$. These tokens are gradually added in the previous sessions. The class-specific tokens X_q^t (Orange) for new classes are concatenated with the old tokens $X_q^{1 \sim t-1}$ (Blue) from the previous in the row dimension, forming the input vectors $X_q \in \mathbb{R}^{|\mathbf{C}^{1 \sim t}| \times D}$:

$$\mathbf{X}_q = [\mathbf{X}_q^1, \dots, \mathbf{X}_q^{t-1}, \mathbf{X}_q^t], \quad X_q^t = \{q_c\}_{|\mathbf{C}^{1 \sim t-1}|+1}^{|\mathbf{C}^{1 \sim t}|} \quad (5)$$

Where the new tokens X_p^t are trainable while the old tokens $X_q^{1 \sim t-1}$ are frozen in the t -th training session. The frozen tokens effectively preserve the knowledge of previous classes to mitigate catastrophic forgetting while simultaneously optimizing the trainable parameters to learn new classes. Then, the patch tokens X_p and class-specific tokens X_q learn attention weights regarding specific embeddings through a multi-head attention mechanism, obtaining class-level embeddings $E \in \mathbb{R}^{|\mathbf{C}^{1 \sim t}| \times D}$, which are then input into the classifier for classification.

To learn new classes, the class-independent classifier also adds $|\mathbf{C}^t|$ Feed Forward Networks (FFNs). Similar to class-specific tokens, FFNs are categorized into two types: frozen FFNs $\varphi(\cdot; \phi_1), \dots, \varphi(\cdot; \phi_{|\mathbf{C}^{1 \sim t-1}|})$ and trainable FFNs $\varphi(\cdot; \phi_{|\mathbf{C}^{1 \sim t-1}|+1}), \dots, \varphi(\cdot; \phi_{|\mathbf{C}^{1 \sim t}|})$. These serve the purpose of maintaining old knowledge and learning new knowledge. Ultimately, the image’s classification loss \mathcal{L}_{ce} is calculated based on the predicted probabilities from each FFN.

D. The Loss Function of CLIN

After introducing the structure of the CLIN method, we proceed to discuss the loss functions that optimize the CLIN method. To address the feature confusion problem, we introduce two terms in the loss function to optimize the learning of

class-level embeddings and class-specific tokens: multi-label contrastive loss and token orthogonal loss. Additionally, similar to previous approaches, our loss function includes base losses, such as classification loss and distillation loss, aiming to achieve the classification task and prevent catastrophic forgetting.

Multi-label Contrastive Loss: In contrast to regular supervised learning on independently and identically distributed data, continual learning faces challenges such as poor discriminative ability in non-stationary data distribution. To address this issue, regular supervised learning methods often employ techniques like metric learning [72] and contrastive learning [73]. Since image-level features are associated with multiple labels, *directly applying* them to multi-label tasks is challenging. For example, assuming that the image-level representation of an image containing a **car** must always be close to each other is unreasonable because the **car** is just one of many objects in these images, possibly occupying only a small part of the image. However, in our CLIN approach, we tackle this problem by using attention mechanisms to transform image features into class-level features, effectively **converting** the *multi-label problem* into multiple *single-label problems*. Furthermore, we propose a *multi-label contrastive loss* to force the model to learn diverse and discriminative features for new concepts, further addressing the feature confusion problem.

First, after obtaining $E \in \mathbb{R}^{|\mathbf{C}| \times D}$, we use $e_c \in \mathbb{R}^D$ to represent the class-level embedding of the input image in the context of a specific class c . Then we introduce a projection layer $\text{Proj}(\cdot)$, which maps e_c to a vector in another embedding space: $z_c = \text{proj}(e_c) \in \mathbb{R}^D$ and we apply the multi-label contrastive loss \mathcal{L}_{mc} in the projected space.

Specifically, in the t -th session, given a small batch N of images $X^t = \{x_i^t \in \mathbf{D}^t \mid i \in \{1, \dots, N\}\}$ (we omit the superscript t in the following text as it is unrelated to session). We first input them into the class-level cross-attention module and the projection layer, obtaining class-level embeddings in the mapped space and defining them as the set $Z = \{z_{ic} \in \mathbb{R}^D \mid i \in \{1, \dots, N\}; c \in \{1, \dots, |\mathbf{C}|\}\}$. Similarly, we define the set of ground truth labels of the minibatch: $Y = \{y_{ic} \in \{0, 1\} \mid i \in \{1, \dots, N\}; c \in \{1, \dots, |\mathbf{C}|\}\}$. It’s worth noting that we consider the class-level embedding z_{ic} of an image as an instance rather than the image itself; z_{ic} is associated with a single true label y_{ic} . We further define $A = \{\{a_k, y_k\} \mid \{z_{ic} \in Z \text{ and } y_{ic} = 1\}\}$ as the instance set containing class-level embeddings, where a_k represents the k -th instance in A , y_k represents the label of a_k , and $y_k = c$.

For pairs of class-level embeddings a_k and a_m , which are randomly selected from the instance set A . Our inter-class objective enforces the following loss on the model:

$$\mathcal{L}_{mc} = \frac{1}{|A|} \sum_{k=1}^{|A|} \sum_{m=1}^{|A|} (1 - \cos(a_k, a_m)) * B_{km}. \quad (6)$$

where $\cos(a_k, a_m)$ denotes the cosine similarity between two class-level embedding a_k and a_m . B_{km} represents the relationship of a_k and a_m . If a_k and a_m represent the same category, i.e., $y_k = y_m$, then $B_{km} = 1$; otherwise, $B_{km} = -1$. The objective of our \mathcal{L}_{mc} loss function is to promote feature distinctiveness among different classes, facilitating diversity in

class-specific knowledge and clustering features belonging to the same class.

Token Orthogonal Loss: In the class-level cross-attention module, the class-specific tokens expand gradually based on the number of classes. To prevent interference between learning new knowledge and old knowledge while enhancing the model’s ability to learn diverse concepts and foster class-specific distinctions for retaining knowledge, we propose addressing this issue through appropriate initialization and a specific loss function.

We apply the Gram-Schmidt process to initialize new token parameters at the beginning of each new session. Certainly, at the t -th session, $|\mathbf{C}^t|$ class-specific tokens X_q^t are introduced. Each new token undergoes the Gram-Schmidt process to ensure that the initialized parameters are orthogonal to the parameters of all the old tokens. This process ensures that the new class-specific tokens are linearly independent from the previously existing tokens. This helps maintain diversity and prevents interference between the representations of different classes, facilitating effective learning and discrimination.

Additionally, we employ a token orthogonal loss to maintain orthogonality between trainable tokens (new classes) and frozen tokens (old classes). In the session $t > 1$, the token orthogonal loss compels the model to optimize new class tokens X_q^t (Orange) to be orthogonal to previous tokens $X_q^{1 \sim t-1} = [X_q^1, X_q^2, \dots, X_q^{t-1}]$ (Blue). This constraint can be formulated as follows:

$$\mathcal{L}_{to} = \|[X_q^1, \dots, X_q^{t-1}] \cdot (X_q^t)^T\| \quad (7)$$

where $\|\cdot\|$ represents the L_2 -norm and T represents the matrix transpose. The \mathcal{L}_{to} serves to continually diminish the mutual influence between new and old class tokens throughout the training process, thereby emphasizing the distinctions between old and new classes.

Base Loss: The base loss function consists of two portions: (1) the classification loss \mathcal{L}_{ce} , an asymmetric loss [61], used to classify the data:

$$\mathcal{L}_{ce} = \frac{1}{N} \sum_{n=1}^N \begin{cases} (1 - p_c)^{\gamma+} \log(p_c), & y_c = 1, \\ p_c^{\gamma-} \log(1 - p_c), & y_c = 0, \end{cases} \quad (8)$$

In the formulation, y_c represents the binary label indicating whether the image has the label c . The parameters $\gamma+$ and $\gamma-$ are positive and negative focusing parameters, respectively.

(2) The distillation loss function \mathcal{L}_{kd} is applied on the class-level embedding layer to prevent the forgetting of old knowledge:

$$\mathcal{L}_{kd} = \|E^{t-1}, \hat{E}^t\|, \quad (9)$$

where E^{t-1} is the class-level embeddings of the old backbone, \hat{E}^t is the class-level embedding of the old classes in the current backbone ($\hat{E}^t = E^t[e_1, \dots, e_{|C^{1 \sim t-1}|}]$), and $\|\cdot\|$ represents the L_2 -norm.

Total Optimization Objective: For session t ($t > 1$), our full optimization consists of the two portions: (1) the separation loss includes the multi-label contrastive loss \mathcal{L}_{mc} and token orthogonal loss \mathcal{L}_{to} . (2) the base loss includes the classification

loss \mathcal{L}_{ce} and distillation loss \mathcal{L}_{kd} . We can obtain the total loss function:

$$\mathcal{L} = \mathcal{L}_{ce} + \alpha * \mathcal{L}_{mc} + \beta * \mathcal{L}_{kd} + \lambda * \mathcal{L}_{to}. \quad (10)$$

where α , β and λ are hyper-parameters. The details are added to the experiments.

IV. EXPERIMENTS

In this section, we conduct extensive experiments to validate the effectiveness of our algorithm, particularly by evaluating its performance on the MS-COCO [74] and PASCAL VOC 2007 [75] datasets using two widely recognized benchmark protocols [11], [12]. Additionally, we delve into a series of ablation studies and visualizations aimed at assessing the importance of each component, providing deeper insights into the workings of our method. The section is structured as follows: we begin by introducing the experimental setup and implementation details in Sec. IV-A. Subsequently, we present the experimental results on the two protocols in Sec. IV-B. Finally, we introduce the ablation study and provide a comprehensive analysis of our method in Sec. IV-C.

A. Experimental Setup and Implementation Details

Dataset. MS-COCO [74] is a large-scale dataset constructed for segmentation and object detection tasks first and has been widely used for evaluating MLC. It contains 122,218 RGB images of 80 object categories, where each class has 82,081 images in the training set and 40,137 images in the validation set. PASCAL VOC [75] is a frequently used dataset for MLC and consists of 9,963 images for 20 object categories, where 5,011 images are in the train-value set, and 4,952 images are in the test set.

Benchmark Protocols. We conduct comprehensive experiments on two popular benchmark protocols [11], [12]. The first protocol is derived from the approach outlined in [11]: arranging class names in alphabetical order and then partitioning the training set into multiple incremental sessions based on the order of categories. While different sessions may include the same images, they come with different provided labels. For the division of incremental phases, we adopt protocols commonly used in CIL [24], [26]. Specifically, for the MS-COCO benchmark, we define it as COCO-B0CX and COCO-B40CY, where B represents the number of base classes, and CX(Y) denotes the addition of X(Y) new class categories during the incremental sessions (X=10, 20, and Y=5, 10). The B0 presents a more challenging scenario. Similarly, for the VOC benchmark, we evaluate our method using the B0-C4 and B10-C2 protocols (denoted as COCO and VOC).

The second protocol is based on [12], where the training set is initially sorted using a random seed (1998). Subsequently, all training data is directly partitioned based on the tasks. It’s important to note that images in different sessions are entirely non-overlapping, although there may be unlabeled images. This protocol can be denoted by a unified terminology Bi-Cj, where i represents the class number to be learned in the base session, and j is the class number to be learned in each incremental session. We assess the models on the Split-COCO dataset with

TABLE I: Main class-incremental results on MS-COCO dataset. Compared methods are grouped based on different buffer sizes. Buffer Size 0 means no rehearsal is required, where most SOTA CIL methods are not applicable anymore. All the input size is 224×224 and all metrics are in %. All compared results are obtained from KRT [11]

Method	Source Task	Buffer Size	MS-COCO B0-C10				MS-COCO B40-C10			
			Avg. Acc	Last Acc			Avg. Acc	Last Acc		
			mAP	CF1	OF1	mAP	mAP	CF1	OF1	mAP
Upper-bound	Baseline	-	-	76.4	79.4	81.8	-	76.4	79.4	81.8
FT [61]	Baseline	0	38.3	6.1	13.4	16.9 (↓ 54.5)	35.1	6.0	13.6	17.0 (↓ 58.3)
PODNet [23]	CIL		43.7	7.2	14.1	25.6 (↓ 45.8)	44.3	6.8	13.9	24.7 (↓ 50.6)
oEWC [36]	CIL		46.9	6.7	13.4	24.3 (↓ 47.1)	44.8	11.1	16.5	27.3 (↓ 48.0)
LWF [38]	CIL		47.9	9.0	15.1	28.9 (↓ 42.5)	48.6	9.5	15.8	29.9 (↓ 45.4)
KRT [11]	MLCIL		74.6	55.6	56.5	65.9 (↓ 5.5)	77.8	64.4	63.4	74.0 (↓ 1.3)
Ours	MLCIL		78.1	61.2	61.1	71.4 (↓ 0.0)	79.0	65.2	64.9	75.3 (↓ 0.0)
TPCIL [22]	CIL	5/class	63.8	20.1	21.6	50.8 (↓ 21.8)	63.1	25.3	25.1	53.1 (↓ 23.0)
PODNet [23]	CIL		65.7	13.6	17.3	53.4 (↓ 19.2)	65.4	24.2	23.4	57.8 (↓ 18.3)
DER++ [24]	CIL		68.1	33.3	36.7	54.6 (↓ 18.0)	69.6	41.9	43.7	59.0 (↓ 17.1)
KRT [11]	MLCIL		75.8	60.0	61.0	68.3 (↓ 4.3)	78.0	66.0	65.9	74.3 (↓ 1.8)
Ours	MLCIL	78.6	63.9	63.9	72.6 (↓ 0.0)	79.2	66.9	67.9	76.1 (↓ 0.0)	
iCaRL [6]	CIL	20/class	59.7	19.3	22.8	43.8 (↓ 30.7)	65.6	22.1	25.5	55.7 (↓ 21.4)
BiC [28]	CIL		65.0	31.0	38.1	51.1 (↓ 23.4)	65.5	38.1	40.7	55.9 (↓ 21.2)
ER [25]	CIL		60.3	40.6	43.6	47.2 (↓ 27.3)	68.9	58.6	61.1	61.6 (↓ 15.5)
TPCIL [22]	CIL		69.4	51.7	52.8	60.6 (↓ 13.9)	72.4	60.4	62.6	66.5 (↓ 10.6)
PODNet [23]	CIL		70.0	45.2	48.7	58.8 (↓ 15.7)	71.0	46.6	42.1	64.2 (↓ 12.9)
DER++ [24]	CIL		72.7	45.2	48.7	63.1 (↓ 11.4)	73.6	51.5	53.5	66.3 (↓ 10.8)
KRT [11]	MLCIL		76.5	63.9	64.7	70.2 (↓ 4.3)	78.3	67.9	68.9	75.2 (↓ 1.9)
Ours	MLCIL		79.5	66.6	67.9	74.5 (↓ 0.0)	79.7	69.8	71.4	77.1 (↓ 0.0)

B40-C10 and B0-C20 protocols and on the Split-VOC dataset with B10-C5 and B0-C5 protocols (denoted as Split-COCO and Split-VOC).

Compared Method. Our method was compared to multiple SOTA continual learning methods following the MLCIL protocol. This included the SOTA MLCIL methods KRT [11] and APPLE [12], along with various single-label class-incremental learning methods for comparison. These single-label methods comprised regularization-based approaches such as EWC [36], LwF [38], and rehearsal-based methods like ER [?], TPCIL [22], DER++ [24], and PODNet [23]. Additionally, we considered prompt-based methods L2P [7] and DualPrompt [17], both utilizing pre-trained ViT-B models and representing the latest SOTA methods in the incremental learning field. The Upper-bound joint trains all classes simultaneously. However, it is not an Incremental Learning (IL) method but serves as an upper bound for performance comparison.

Evaluation metrics. Following the precedent set by prior incremental learning studies [11], [26], [47], we report two key metrics, average accuracy and final accuracy. For a comprehensive evaluation of all learned categories within each session, we utilize the mean average precision (mAP) and report both the average mAP (the mean of the mAP across all sessions) and the final mAP (mAP in the final session). To further enhance the evaluation of performance across all incremental tasks, we include the per-class F1 measure (CF1) and overall F1 measure (OF1) alongside the final accuracy.

Implementation details. All methods were implemented using PyTorch and trained on 2 RTX 3090 GPUs. We employed a TRResNetM backbone pre-trained on ImageNet-21k (L2P [7] and Dual-prompt utilized ViT-B/16 pre-trained on ImageNet-21k as the backbone). The input resolution is set to $h \times w = 224 \times 224$ or $h \times w = 448 \times 448$ depending on the training protocol. The projection dimension D and hidden dimension l of the CINet module were configured as 768. Our method was trained for 20 epochs using the Adam optimizer and OneCycleLR scheduler, with a weight decay of 1×10^{-4} . The batch size was set to 64. For training the base model, the learning rate was set to 4×10^{-5} . During the incremental sessions, we set the learning rate to 1×10^{-4} for COCO and 8×10^{-5} for VOC. For the hyperparameters of total optimization, α is typically set to 0.05, β is set to 80, and λ is 0.1. Data augmentation techniques included rand augmentation and cutout. Additionally, we conducted experiments three times and reported the average results.

B. Comparison with State-of-the-arts.

Result on COCO benchmark: Tab I presents the results of the MS-COCO B0-C10 and B40-C10 benchmark. Our method consistently outperforms all comparison methods in terms of average accuracy (mAP) and final accuracy (CF1, OF1, and mAP). Specifically, when the buffer size is larger (20 per class), our method achieves the best final accuracies of **74.5%** and **77.1%** on the two benchmarks, surpassing SOTA CIL methods by **11.4%** and **10.6%**, respectively. It also outperforms the

TABLE II: Class-incremental results on MS-COCO and PASCAL VOC datasets. Compare methods under different protocols against comparison methods. All the input size is 224×224 .

Method	Buffer Size	MS-COCO B0-C20		MS-COCO B40-C5		Buffer Size	VOC B0-C4		VOC B10-C2	
		Avg. Acc	Last Acc	Avg. Acc	Last Acc		Avg. Acc	Last Acc	Avg. Acc	Last Acc
		mAP (%)	mAP (%)	mAP (%)	mAP (%)		mAP (%)	mAP (%)	mAP (%)	mAP (%)
Upper-bound	-	-	81.8	-	81.8	-	-	93.6	-	93.6
FT [61]	0	51.4	27.0 (↓ 49.7)	24.5	10.7 (↓ 58.2)	0	82.4	62.9 (↓ 21.1)	70.1	43.0 (↓ 31.3)
KRT [11]		79.4	74.8 (↓ 1.9)	73.5	65.4 (↓ 3.5)		89.1	80.2 (↓ 3.8)	84.3	71.5 (↓ 2.8)
Ours		80.7	76.7 (↓ 0.0)	75.4	68.9 (↓ 0.0)		91.1	84.0 (↓ 0.0)	85.6	74.3 (↓ 0.0)
iCaRL [6]	20/class	69.0	52.4 (↓ 24.6)	62.4	53.9 (↓ 20.6)	2/class	87.2	72.4 (↓ 14.0)	79.0	66.7 (↓ 16.8)
BiC [28]		70.3	51.5 (↓ 25.5)	60.2	51.7 (↓ 22.8)		86.8	72.2 (↓ 14.2)	81.7	69.7 (↓ 13.8)
ER [25]		68.7	58.0 (↓ 19.0)	65.5	58.1 (↓ 16.4)		86.1	71.5 (↓ 14.9)	81.5	68.6 (↓ 14.9)
TPCIL [22]		73.2	63.4 (↓ 13.6)	69.5	64.2 (↓ 10.3)		87.6	77.3 (↓ 9.1)	80.7	70.8 (↓ 12.7)
PODNet [23]		74.9	66.9 (↓ 10.1)	66.8	58.9 (↓ 15.6)		88.1	76.6 (↓ 9.8)	81.2	71.4 (↓ 12.1)
DER++ [24]		75.9	68.2 (↓ 8.8)	68.9	62.1 (↓ 12.4)		87.9	76.1 (↓ 10.3)	82.3	70.6 (↓ 12.9)
KRT [11]		79.4	75.2 (↓ 1.8)	76.3	72.4 (↓ 2.1)		90.7	83.4 (↓ 3.0)	87.7	80.5 (↓ 3.0)
Ours		80.8	77.0 (↓ 0.0)	78.2	74.5 (↓ 0.0)		92.4	86.4 (↓ 0.0)	90.3	83.5 (↓ 0.0)

TABLE III: Class-Incremental results (mAP%) on MS-COCO dataset against prompt-based CIL method. ∇ indicates the gap towards the Upper Bound of the corresponding backbone. All the input size is 224×224 and all metrics are in %.

Method	Backbone	Param.	MS-COCO B10-C10		MS-COCO B40-C10	
			Avg. Acc	Last Acc	Avg. Acc	Last Acc
Upper-bound			-	83.16	-	83.16
L2P [7]	ViT-B/16	86.0M	73.28 (↓ 6.23)	67.72 (∇ 15.44)	73.07 (↓ 6.66)	70.42 (∇ 12.74)
L2P-R [7]			73.87 (↓ 5.64)	68.22 (∇ 14.94)	73.64 (↓ 6.09)	71.68 (∇ 11.48)
Dual-prompt [17]			74.67 (↓ 4.84)	69.39 (∇ 13.77)	74.45 (↓ 5.28)	71.95 (∇ 11.21)
Dual-prompt-R [7]			74.87 (↓ 4.64)	70.20 (∇ 12.96)	74.54 (↓ 5.19)	72.60 (∇ 10.56)
Upper-bound					-	81.80
KRT [11]	TResNetM	29.4M	74.64 (↓ 4.87)	65.94 (∇ 15.86)	77.83 (↓ 1.90)	74.02 (∇ 7.78)
KRT-R [11]			76.53 (↓ 2.98)	71.24 (∇ 10.56)	78.34 (↓ 1.39)	75.18 (∇ 6.62)
Our			78.14 (↓ 1.37)	71.36 (∇ 10.44)	78.99 (↓ 0.74)	75.32 (∇ 6.48)
Our-R			79.51 (↓ 0.00)	74.47 (∇ 7.33)	79.73 (↓ 0.00)	77.14 (∇ 4.66)

latest MLCIL method, KRT, by **4.3%** and **1.9%**. When the buffer size decreases (5 per class), our shows larger performance gains compared to other continuals. Notably, when the buffer size is set to 0, our maintains superior performance, far exceeding regularization-based methods and other rehearsal-based methods, with improvements of **42.5%** and **45.8%** on the B0-C10 benchmark, respectively. Furthermore, our method is more suitable for rehearsal-free scenarios. Specifically, under the B0-C10 protocol, our method achieves average and final accuracy of **78.1%** and **71.4%**, respectively, compared to KRT (buffer size=0), representing improvements of **3.5%** and **5.5%**, and even outperforming KRT-R (buffer size=20) by **1.6%** and **1.2%**.

Tab II demonstrates the results for the other two benchmarks of COCO, including B0-C20 and B40-C5. Similar to the previous benchmarks of COCO, our method achieves the best accuracy across multiple metrics. Specifically, it attains final accuracies of **77.0%** and **74.5%** on the two benchmarks, outperforming rehearsal-based methods by at least **8.8%** and **10.3%**. Additionally, we observe improvements compared to the KRT method, especially when the buffer size is set to 0. Furthermore, under the relatively simpler protocols, our final

accuracy has reached **77.0%**, approaching the upper bound of **81.8%**, highlighting the effectiveness of our method.

The current SOTA methods in SLCIL are prompt-based approaches. These methods, based on the ViT-B pre-trained model and utilizing prompts, demonstrate powerful capabilities in preventing catastrophic forgetting. For a more comprehensive comparison, we not only evaluate our method on the B40-C10 on the COCO dataset but also the more challenging B0-C10. As prompt-based methods use a different backbone model compared to our approach, we use the tendency toward an upper bound (∇) to measure the performance of each method given a specific backbone. Table III illustrates the comparison between our method and prompt-based methods. We observe that our method consistently outperforms prompt-based methods comprehensively, with higher performance across all scenarios, both with and without buffer, compared to the KRT method. Specifically, our approach shows gaps of **7.33%** and **4.66%** compared to the upper bound, while DualPrompt exhibits gaps of **12.96%** and **10.56%** compared to the upper bound. In comparison to the Prompt method, we achieve improvements of at least **5.63%**. It is worth noting that despite our method having a lower upper bound, the average accuracy on the two

TABLE IV: Experimental results (mAP%) of our method and comparison methods on Split-COCO and Split-VOC datasets. All the input size is 448×448 , and all metrics are in %. All compared results are obtained from APPLE [12]

Methods	Buffer Size	Split-COCO B40-C10		Split-COCO B0-C20		Buffer Size	Split-VOC B10-C5		Split-VOC B0-C5	
		Avg. Acc	Last Acc	Avg. Acc	Last Acc		Avg. Acc	Last Acc	Avg. Acc	Last Acc
Upper bound	-	-	86.43	-	86.43	-	-	94.18	-	94.18
FT	0/class	35.83	11.12 (↓ 71.92)	51.87	23.60 (↓ 58.93)	0/class	74.82	60.09 (↓ 32.26)	74.10	59.73 (↓ 30.53)
Ours	0/class	84.36	82.54 (↓ 0.50)	83.39	81.71 (↓ 0.82)	0/class	94.66	91.98 (↓ 0.37)	93.88	89.45 (↓ 0.81)
iCaRL [6]	20/class	76.69	65.60 (↓ 17.44)	76.53	64.54 (↓ 17.41)	5/class	90.78	87.07 (↓ 5.28)	88.33	84.78 (↓ 5.48)
ER [25]		72.30	64.05 (↓ 18.99)	63.59	50.14 (↓ 32.81)		86.01	73.91 (↓ 18.44)	82.68	68.31 (↓ 21.95)
TPCIL [22]		69.41	71.20 (↓ 11.84)	73.54	68.89 (↓ 14.06)		90.19	84.18 (↓ 8.17)	87.95	79.38 (↓ 10.88)
PODNet [23]		77.11	66.12 (↓ 16.92)	74.78	61.01 (↓ 21.94)		90.35	86.35 (↓ 6.00)	87.78	84.12 (↓ 6.14)
PASS [76]		73.80	59.44 (↓ 23.60)	72.16	49.88 (↓ 33.07)		86.01	76.93 (↓ 15.42)	75.58	51.84 (↓ 38.42)
DER++ [24]		66.71	55.77 (↓ 27.27)	73.82	67.33 (↓ 15.62)		90.22	83.95 (↓ 8.40)	88.95	84.82 (↓ 5.44)
APPLE [12]		82.05	74.61 (↓ 8.43)	83.49	76.65 (↓ 6.30)		91.68	89.36 (↓ 2.99)	89.52	85.62 (↓ 4.64)
Ours		84.79	83.04 (↓ 0.00)	83.92	82.53 (↓ 0.00)		94.85	92.35 (↓ 0.00)	95.62	90.26 (↓ 0.00)

benchmarks is improved by at least **4.64%**.

Result on VOC benchmark: Tab II summarizes the experimental results on the VOC benchmark. We observe similar trends as seen in the COCO dataset results. Specifically, our method achieves a significant improvement in the final mAP compared to KRT, with an increase of **3.0%** (**83.4%** → **86.4%**) and **3.0%** (**80.5%** → **83.5%**), surpassing other rehearsal methods by at least **9.1%**. It is noteworthy that KRT experiences a significant drop in accuracy on the more challenging benchmark (B10-C2) without a buffer, while our method maintains good accuracy, resulting in a relative improvement of **3.8%**.

Results on Split-COCO and Split-VOC benchmark: Tab IV summarizes the experimental results on the Split-COCO and Split-VOC benchmarks. We observe that our method exhibits significant improvements compared to rehearsal-based methods on these new protocols and achieves higher advancements compared to the SOTA method APPLE in the field of MLCIL. Specifically, our method outperforms APPLE by **8.43%** and **6.30%** on the two benchmarks in Split-COCO and achieves a maximum improvement of **4.64%** on the relatively simpler Split-VOC. Furthermore, even with a buffer size of 0, our method experiences a maximum accuracy drop of only **0.78%**, providing further evidence of the effectiveness of our approach.

C. Ablation Study

Ablation of Different Components: To demonstrate how each component of the proposed CLIN framework contributes to performance improvements, we conducted ablation studies by building five models on MS-COCO under the B0-C10 benchmark: (1) We introduced a distillation loss as the **baseline** model. (2) We added a class-independent incremental Network (CINet) to improve the baseline model. (3) We added both the CINet and the proposed token orthogonal loss \mathcal{L}_{to} to improve the baseline model. (4) We added both the CINet and the proposed multi-label contrastive loss \mathcal{L}_{mc} to improve the baseline model. (5) We added all four components to improve the baseline model.

Table V shows the average mAP and each session mAP of the above models. Specifically, the baseline model produced the lowest last mAP value of **58.4%**. Adopting the CINet improved

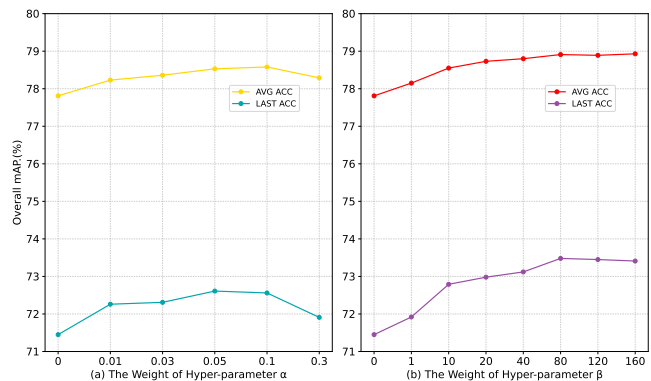


Fig. 3: Comparison of the average and last accuracy with different settings of parameters α and β .

the last mAP by **15.0%**. Adding the token orthogonal loss \mathcal{L}_{to} further improved the performance by **0.6%**. Adding the multi-label contrastive loss \mathcal{L}_{mc} further improved the performance by **1.0%**. The final model, which consists of all three components, achieved the best average mAP and last mAP of **79.5%** and **74.5%**. These experimental results strongly demonstrate that the three components utilized in the proposed CLIN method are highly effective in preventing forgetting and improving performance for MLCIL tasks.

Sensitive Study of Hyper-parameter: The hyper-parameters α , β and λ control the strength of \mathcal{L}_{mc} , \mathcal{L}_{kd} and \mathcal{L}_{to} to together control the total optimization objective.

We first conducted a sensitivity study on α using the COCO B0-C10 benchmark, where we changed the value of α in the reasonable range of $\{0, 0.01, 0.03, 0.05, 0.1, 0.3\}$, respectively. The results are shown in Fig 4, and we observed that with the increase of α , the final accuracy and average accuracy consistently improved, reaching the optimal final accuracy of **72.56%** at $\alpha=0.05$, representing a relative improvement of **1.11%**. Subsequently, as α continued to increase, the rate of performance improvement gradually decreased. The experimental trends align with expectations. In contrast to single-label classification, label correlation is crucial in multi-label classification. For instance, when we observe a **tennis ball**

TABLE V: The effectiveness of CLIN’s different components in performance improvements.

Baseline	CINet	TO loss	MC loss	Acc (mAP%) in each session								Avg. Acc
				1	2	3	4	5	6	7	8	
✓				92.5	79.5	73.0	67.8	62.7	62.6	59.9	58.4 (↑ 0.0)	69.5
✓	✓			92.6	83.0	79.4	77.3	76.0	75.3	73.8	73.4 (↑ 15.0)	78.9
✓	✓	✓		92.8	83.5	79.9	77.4	76.1	75.9	74.3	74.0 (↑ 15.6)	79.2
✓	✓		✓	93.0	83.3	79.7	77.5	76.3	76.0	74.5	74.4 (↑ 16.0)	79.3
✓	✓	✓	✓	92.9	83.3	79.8	77.9	76.8	76.2	74.6	74.5 (↑ 16.1)	79.5

in an image, we can assume a high probability of the **tennis racket** appearing in the image as well. Therefore, categories in the embedded space should not be overly separated.

To validate the robustness and effectiveness of the CLIN approach, we conducted experiments with different weights of hyper-parameter β on COCO B0-C10. Specifically, we tested β values of 0, 1, 10, 20, 40, 80, 120, and 160, respectively. The comparative results are shown in Fig. 4. We observed that our method achieved the best final performance of **73.47%** when β was set to 80. Furthermore, our method demonstrated a small performance range across different β parameters, ranging from **71.49%** to **73.42%**, confirming the model’s robustness to variations in the β parameter. At the same time, we observed that even without distillation loss, our CLIN framework achieved a minimum final accuracy of **71.49%**, with only a relative decrease of **1.93%**. This demonstrates the effectiveness of our structural design in mitigating catastrophic forgetting.

TABLE VI: Sensitive study of hyper-parameter λ .

λ	0	0.0001	0.001	0.01	0.1	1	10
Last Acc (%)	71.49	71.55	71.62	72.05	72.18	72.10	71.86

We finally conducted a sensitivity study on λ using the same benchmark, where we changed the value of λ in the reasonable range from 0.0001 to 10. From Table VI, it can be observed that as λ increases, the final mAP(%) gradually improves and reaches the highest accuracy **72.18%** at 0.1. However, further increases in λ indicate that excessively strong regularization constraints can impact other loss functions.

TABLE VII: Compare different methods on MS-COCO with different numbers of exemplars M_{per} per class.

Method		M_{per}				
		0	5	10	20	30
PodNet* [23]	Last Acc	25.6	53.4	55.6	58.8	59.0
	Avg Acc	43.7	65.7	66.8	70.0	70.3
KRT [11]	Last Acc	65.9	68.3	69.4	70.2	71.5
	Avg Acc	74.6	75.8	76.4	76.5	77.3
Ours	Last Acc	71.4	72.6	73.4	74.5	75.1
	Avg Acc	78.1	78.6	79.1	79.4	79.8

The Influence of Buffer Size: Incremental Learning methods typically utilize additional memory space to store a fixed number of exemplars per old class, denoted as (M_{per}), to mitigate catastrophic forgetting. Intuitively, retaining more exemplars may enhance recognition performance but also come

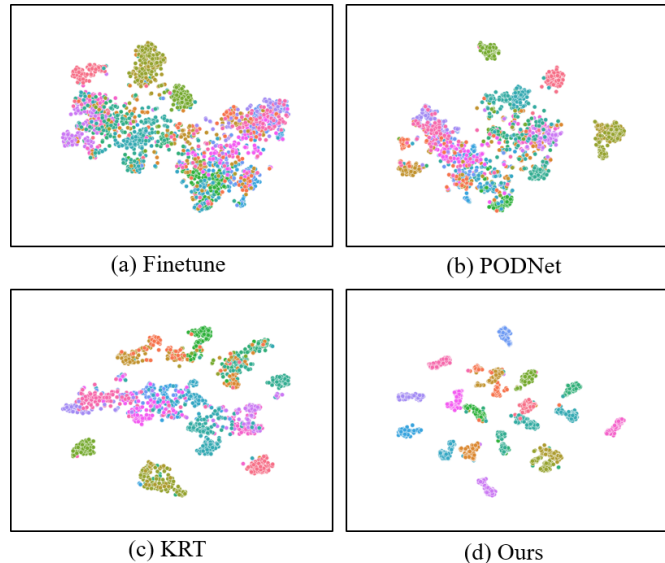


Fig. 4: Comparison of t-SNE visualizations between other methods and our approach, where each color represents a category.

with a greater memory burden. Therefore, it is valuable to compare our approach against the rehearsal-based methods PodNet [23] and the SOTA method KRT [11] with different numbers of exemplars in the MS-COCO with B0-C10 setting (refer to Table VII).

We observe that our method consistently outperforms PodNet* and KRT, achieving a final accuracy of **74.5%**. As the number of exemplars (M_{per}) decreases, the advantage of our method continues to grow. Specifically, with an ample buffer of $M_{per} = 30$, our method outperforms KRT by **3.6%** in final accuracy. Moreover, in the scenario with no old examples ($M_{per} = 0$), our method exhibits a remarkable improvement of **5.5%**. This implies that CLIN does not rely on the storage of old examples. It is noteworthy that when the $M_{per} = 0$, the accuracy of the rehearsal-based method is seriously attenuated and our method significantly outperforms PodNet* by **45.8%** (**25.6%** \rightarrow **71.4%**) on last accuracy.

Visualization of CLIN Method: To demonstrate that the CLIN approach effectively addresses category confusion issues, we conducted t-SNE visualizations on the final models of various methods under the COCO B0C10 protocol, focusing on the earliest learned 0-20 classes. Through visualization, the observations are as follows: (a) Finetune methods exhibit severe category confusion, leading to significant catastrophic forgetting

issues. (b,c) The visualizations of the Rehearsal-based method PODNet and NE-based method KRT show some boundaries between categories compared to the Finetune method. However, the features of different classes remain highly confusing. This indicates that global or task-level features alone cannot resolve confusion issues, resulting in catastrophic forgetting problems. (d) Our CLIN method, through the CINet and proposed loss functions, effectively resolves category confusion in multi-label class incremental learning. The visualization demonstrates clear distinctions between different classes, validating the effectiveness and rationality of our approach.

V. CONCLUSION

This paper primarily investigates the problem of multi-label class-incremental learning. We propose an effective Continual Class-Independent (CLIN) framework to address the challenges of inter-session confusion and the unique intra-feature confusion associated with MLCIL tasks. Firstly, the proposed CINet combines attention mechanisms with scalable class-specific tokens. It effectively generates and processes class-level features to address confusion problems while preserving knowledge for each old class through a small number of parameters independent of the shared model. Secondly, the CINet transforms the multi-label problem into a single-label problem. On this basis, two loss functions are proposed to optimize class-specific tokens and class-level embeddings. In terms of experiments, the performance of the CLIN method consistently outperformed other SOTA methods, particularly in scenarios where no buffer storage was used. We also conducted detailed ablation experiments and visual analyses to demonstrate the effectiveness of the proposed modules and loss functions.

Limitation and Feature work. This paper explores and addresses the task of MLCIL from the perspective of incremental learning and has achieved promising results. In terms of label correlation, it attempts to use a Transformer decoder to extract local discriminative features for different labels and establish co-occurrence relationships between categories. However, it does not delve into the contribution of label dependencies in preventing forgetting and learning new classes. Moreover, due to the insensitivity to algorithm time complexity in incremental learning tasks, our paper does not discuss it.

In the future, we will further (1) investigate the co-occurrence relationship between labels in the query ((token))-to-label structure, using label dependencies as knowledge retention to prevent forgetting and to enhance multi-label classification performance. (2) Investigate the impact of unlearned potential categories in images on the task. (3) Extend the approach to more network frameworks, such as large-scale natural language models like CLIP and other multi-label application scenarios.

REFERENCES

- [1] L. Song, J. Liu, B. Qian, M. Sun, K. Yang, M. Sun, and S. Abbas, "A deep multi-modal cnn for multi-instance multi-label image classification," *IEEE Transactions on Image Processing*, vol. 27, no. 12, pp. 6025–6038, 2018. 1
- [2] J. Zhang, J. Ren, Q. Zhang, J. Liu, and X. Jiang, "Spatial context-aware object-attentional network for multi-label image classification," *IEEE Transactions on Image Processing*, 2023. 1, 3
- [3] L. Jing, Y. Chen, and Y. Tian, "Coarse-to-fine semantic segmentation from image-level labels," *IEEE transactions on image processing*, vol. 29, pp. 225–236, 2019. 1
- [4] S. Deng, S. Li, K. Xie, W. Song, X. Liao, A. Hao, and H. Qin, "A global-local self-adaptive network for drone-view object detection," *IEEE Transactions on Image Processing*, vol. 30, pp. 1556–1569, 2020. 1
- [5] J. U. Kim, H.-I. Kim, and Y. M. Ro, "Stereoscopic vision recalling memory for monocular 3d object detection," *IEEE Transactions on Image Processing*, 2023. 1
- [6] S.-A. Rebuffi, A. Kolesnikov, G. Sperl, and C. H. Lampert, "icarl: Incremental classifier and representation learning," in *CVPR*, 2017, pp. 2001–2010. 1, 2, 8, 9, 10
- [7] Z. Wang, Z. Zhang, and et al., "Learning to prompt for continual learning," in *CVPR*, 2022, pp. 139–149. 1, 3, 8, 9
- [8] Z. Ji, Z. Hou, X. Liu, Y. Pang, and X. Li, "Memorizing complementation network for few-shot class-incremental learning," *IEEE Transactions on Image Processing*, vol. 32, pp. 937–948, 2023. 1
- [9] K. Li, J. Wan, and S. Yu, "Ckdf: Cascaded knowledge distillation framework for robust incremental learning," *IEEE Transactions on Image Processing*, vol. 31, pp. 3825–3837, 2022. 1, 2
- [10] Z. Ji, J. Li, Q. Wang, and Z. Zhang, "Complementary calibration: Boosting general continual learning with collaborative distillation and self-supervision," *IEEE Transactions on Image Processing*, vol. 32, pp. 657–667, 2022. 1
- [11] S. Dong, H. Luo, Y. He, X. Wei, J. Cheng, and Y. Gong, "Knowledge restore and transfer for multi-label class-incremental learning," in *Proceedings of the IEEE/CVF International Conference on Computer Vision*, 2023, pp. 18711–18720. 1, 2, 4, 7, 8, 9, 11
- [12] X. Song, K. Shu, S. Dong, and X. Wei, "Overcoming catastrophic forgetting for multi-label class-incremental learning," *IEEE Winter Conference on Applications of Computer Vision*, 2023. 1, 2, 4, 7, 8, 10
- [13] Y.-S. Liang and W.-J. Li, "Optimizing class distribution in memory for multi-label online continual learning," *arXiv preprint arXiv:2209.11469*, 2022. 1, 4
- [14] C. D. Kim, J. Jeong, and G. Kim, "Imbalanced continual learning with partitioning reservoir sampling," in *Computer Vision—ECCV 2020: 16th European Conference, Glasgow, UK, August 23–28, 2020, Proceedings, Part XIII 16*. Springer, 2020, pp. 411–428. 1, 4
- [15] K. Du, F. Lyu, F. Hu, L. Li, W. Feng, F. Xu, and Q. Fu, "Agn: augmented graph convolutional network for lifelong multi-label image recognition," in *ICME*. IEEE, 2022, pp. 01–06. 1, 4
- [16] K. Du, F. Lyu, L. Li, F. Hu, W. Feng, F. Xu, X. Xi, and H. Cheng, "Multi-label continual learning using augmented graph convolutional network," *IEEE Transactions on Multimedia*, 2023. 1, 4
- [17] Z. Wang, Z. Zhang, S. Ebrahimi, R. Sun, H. Zhang, C.-Y. Lee, X. Ren, G. Su, V. Perot, J. Dy *et al.*, "Dualprompt: Complementary prompting for rehearsal-free continual learning," in *European Conference on Computer Vision*. Springer, 2022, pp. 631–648. 1, 3, 8, 9
- [18] M. Masana, X. Liu, B. Twardowski, M. Menta, A. D. Bagdanov, and J. Van De Weijer, "Class-incremental learning: survey and performance evaluation on image classification," *IEEE Transactions on Pattern Analysis and Machine Intelligence*, vol. 45, no. 5, pp. 5513–5533, 2022. 2
- [19] S. Liu, L. Zhang, X. Yang, H. Su, and J. Zhu, "Query2label: A simple transformer way to multi-label classification," *arXiv preprint arXiv:2107.10834*, 2021. 2, 3
- [20] J. Lanchantin, T. Wang, V. Ordonez, and Y. Qi, "General multi-label image classification with transformers," in *CVPR*, 2021, pp. 16478–16488. 2, 3
- [21] T. Ridnik, G. Sharir, A. Ben-Cohen, E. Ben-Baruch, and A. Noy, "MI-decoder: Scalable and versatile classification head," in *Proceedings of the IEEE/CVF Winter Conference on Applications of Computer Vision*, 2023, pp. 32–41. 2, 3
- [22] X. Tao, X. Chang, X. Hong, X. Wei, and Y. Gong, "Topology-preserving class-incremental learning," in *ECCV*. Springer, 2020, pp. 254–270. 2, 8, 9, 10
- [23] A. Douillard, M. Cord, and et al., "Podnet: Pooled outputs distillation for small-tasks incremental learning," in *ECCV*. Springer, 2020, pp. 86–102. 2, 8, 9, 10, 11
- [24] P. Buzzega, M. Boschini, A. Porrello, and et al., "Dark experience for general continual learning: a strong, simple baseline," *NIPS*, vol. 33, pp. 15920–15930, 2020. 2, 7, 8, 9, 10
- [25] M. Riemer, I. Cases, and et al., "Learning to learn without forgetting by maximizing transfer and minimizing interference," *arXiv preprint arXiv:1810.11910*, 2018. 2, 8, 9, 10

- [26] S. Hou, X. Pan, C. C. Loy, Z. Wang, and D. Lin, "Learning a unified classifier incrementally via rebalancing," in *CVPR*, 2019, pp. 831–839. 2, 7, 8
- [27] Y. Liu, X. Hong, X. Tao, S. Dong, J. Shi, and Y. Gong, "Model behavior preserving for class-incremental learning," *IEEE Transactions on Neural Networks and Learning Systems*, 2022. 2
- [28] Y. Wu, Y. Chen, L. Wang, Y. Ye, Z. Liu, Y. Guo, and Y. Fu, "Large scale incremental learning," in *CVPR*, 2019, pp. 374–382. 2, 8, 9
- [29] B. Zhao, X. Xiao, G. Gan, B. Zhang, and S.-T. Xia, "Maintaining discrimination and fairness in class incremental learning," in *CVPR*, 2020, pp. 13 208–13 217. 2
- [30] E. Belouadah and et al., "Ii2m: Class incremental learning with dual memory," in *ICCV*, 2019, pp. 583–592. 2
- [31] H. Xu and J. Zhang, "Aanet: Adaptive aggregation network for efficient stereo matching," in *CVPR*, 2020, pp. 1959–1968. 2
- [32] Y. Shi, K. Zhou, J. Liang, Z. Jiang, J. Feng, P. H. Torr, S. Bai, and V. Y. Tan, "Mimicking the oracle: An initial phase decorrelation approach for class incremental learning," in *CVPR*, 2022, pp. 16 722–16 731. 2
- [33] A. Ashok, K. Joseph, and et al., "Class-incremental learning with cross-space clustering and controlled transfer," in *ECCV*. Springer, 2022, pp. 105–122. 2
- [34] J. Kirkpatrick, R. Pascanu, N. Rabinowitz, J. Veness, G. Desjardins, A. A. Rusu, K. Milan, J. Quan, T. Ramalho, A. Grabska-Barwinska et al., "Overcoming catastrophic forgetting in neural networks," *National Academy of Sciences*, vol. 114, no. 13, pp. 3521–3526, 2017. 2
- [35] F. Zenke, B. Poole, and S. Ganguli, "Continual learning through synaptic intelligence," in *ICML*. JMLR.org, 2017, pp. 3987–3995. 2, 3
- [36] J. Schwarz, W. Czarnecki, and et al., "Progress & compress: A scalable framework for continual learning," in *ICML*. PMLR, 2018, pp. 4528–4537. 2, 3, 8
- [37] X. Liu, M. Masana, L. Herranz, J. Van de Weijer, A. M. Lopez, and A. D. Bagdanov, "Rotate your networks: Better weight consolidation and less catastrophic forgetting," in *International Conference on Pattern Recognition*. IEEE, 2018, pp. 2262–2268. 3
- [38] Z. Li and D. Hoiem, "Learning without forgetting," *IEEE Transactions on Pattern Analysis and Machine Intelligence*, vol. 40, no. 12, pp. 2935–2947, 2017. 3, 8
- [39] P. Dhar, R. V. Singh, K.-C. Peng, Z. Wu, and R. Chellappa, "Learning without memorizing," in *CVPR*, 2019, pp. 5138–5146. 3
- [40] A. Mallya and S. Lazebnik, "Packnet: Adding multiple tasks to a single network by iterative pruning," in *CVPR*, 2018, pp. 7765–7773. 3
- [41] J. Serra, D. Suris, M. Miron, and et al., "Overcoming catastrophic forgetting with hard attention to the task," in *ICML*. PMLR, 2018, pp. 4548–4557. 3
- [42] A. A. Rusu, N. C. Rabinowitz, G. Desjardins, H. Soyer, J. Kirkpatrick, K. Kavukcuoglu, R. Pascanu, and R. Hadsell, "Progressive neural networks," *arXiv preprint arXiv:1606.04671*, 2016. 3
- [43] S. Yan, J. Xie, and X. He, "Der: Dynamically expandable representation for class incremental learning," in *CVPR*, 2021, pp. 3014–3023. 3
- [44] A. Douillard, A. Ramé, G. Couairon, and M. Cord, "Dytox: Transformers for continual learning with dynamic token expansion," in *CVPR*, 2022, pp. 9285–9295. 3
- [45] Y. Wang, Z. Huang, and X. Hong, "S-prompts learning with pre-trained transformers: An occam's razor for domain incremental learning," *Advances in Neural Information Processing Systems*, vol. 35, pp. 5682–5695, 2022. 3
- [46] K. Shmelkov, C. Schmid, and K. Alahari, "Incremental learning of object detectors without catastrophic forgetting," in *ICCV*, 2017, pp. 3400–3409. 3
- [47] T. Feng, M. Wang, and et al., "Overcoming catastrophic forgetting in incremental object detection via elastic response distillation," in *CVPR*, 2022, pp. 9427–9436. 3, 8
- [48] K. J. Joseph, S. Khan, F. S. Khan, and V. N. Balasubramanian, "Towards open world object detection," in *CVPR*, Jun 2021. [Online]. Available: <http://dx.doi.org/10.1109/cvpr46437.2021.00577> 3
- [49] Y. Liu, B. Schiele, A. Vedaldi, and C. Rupprecht, "Continual detection transformer for incremental object detection," in *CVPR*, 2023, pp. 23 799–23 808. 3
- [50] U. Michieli and P. Zanuttigh, "Continual semantic segmentation via repulsion-attraction of sparse and disentangled latent representations," in *CVPR*, Jun 2021. [Online]. Available: <http://dx.doi.org/10.1109/cvpr46437.2021.00117> 3
- [51] A. Douillard, Y. Chen, and et al., "Plop: Learning without forgetting for continual semantic segmentation," in *CVPR*, Jun 2021. [Online]. Available: <http://dx.doi.org/10.1109/cvpr46437.2021.00403> 3
- [52] S. Cha, Y. Yoo, and et al., "Ssul: Semantic segmentation with unknown label for exemplar-based class-incremental learning," *NIPS*, vol. 34, pp. 10 919–10 930, 2021. 3
- [53] L. Yu, X. Liu, and J. Van de Weijer, "Self-training for class-incremental semantic segmentation," *IEEE Transactions on Neural Networks and Learning Systems*, 2022. 3
- [54] Y. Gong, Y. Jia, T. Leung, A. Toshev, and S. Ioffe, "Deep convolutional ranking for multilabel image annotation," *arXiv preprint arXiv:1312.4894*, 2013. 3
- [55] J. Wang, Y. Yang, J. Mao, Z. Huang, C. Huang, and W. Xu, "Cnn-rnn: A unified framework for multi-label image classification," in *CVPR*, 2016, pp. 2285–2294. 3
- [56] Z. Wang, T. Chen, G. Li, R. Xu, and et al., "Multi-label image recognition by recurrently discovering attentional regions," in *ICCV*, 2017, pp. 464–472. 3
- [57] X. Li, F. Zhao, and Y. Guo, "Multi-label image classification with a probabilistic label enhancement model," in *UAI*, vol. 1, no. 2, 2014, pp. 1–10. 3
- [58] Z. Chen, X.-S. Wei, P. Wang, and Y. Guo, "Learning graph convolutional networks for multi-label recognition and applications," in *TPAMI*, 2021. 3
- [59] T. Wu, Q. Huang, Z. Liu, Y. Wang, and D. Lin, "Distribution-balanced loss for multi-label classification in long-tailed datasets," in *ECCV*. Springer, 2020, pp. 162–178. 3
- [60] T.-Y. Lin, P. Goyal, R. Girshick, K. He, and P. Dollár, "Focal loss for dense object detection," in *ICCV*, 2017, pp. 2980–2988. 3
- [61] T. Ridnik, E. Ben-Baruch, and et al., "Asymmetric loss for multi-label classification," in *ICCV*, 2021, pp. 82–91. 3, 7, 8, 9
- [62] S. You, C. Xu, Y. Wang, C. Xu, and D. Tao, "Streaming label learning for modeling labels on the fly," *arXiv: Machine Learning, arXiv: Machine Learning*, Apr 2016. 3
- [63] W. Liu, H. Wang, X. Shen, and I. W. Tsang, "The emerging trends of multi-label learning," *IEEE transactions on pattern analysis and machine intelligence*, vol. 44, no. 11, pp. 7955–7974, 2021. 3
- [64] Y. Zhu, K. M. Ting, and Z.-H. Zhou, "Multi-label learning with emerging new labels," *IEEE Transactions on Knowledge and Data Engineering*, vol. 30, no. 10, pp. 1901–1914, 2018. 3, 4
- [65] Z. Wang, L. Liu, and D. Tao, "Deep streaming label learning," in *International Conference on Machine Learning*. PMLR, 2020, pp. 9963–9972. 3
- [66] X. Zheng, P. Li, Z. Chu, and X. Hu, "A survey on multi-label data stream classification," *IEEE Access*, vol. 8, pp. 1249–1275, 2019. 3
- [67] Y. Zhang, Y. Wang, X.-Y. Liu, S. Mi, and M.-L. Zhang, "Large-scale multi-label classification using unknown streaming images," *Pattern Recognition*, vol. 99, p. 107100, 2020. 3
- [68] J. Liu, Y. Li, W. Weng, J. Zhang, B. Chen, and S. Wu, "Feature selection for multi-label learning with streaming label," *Neurocomputing*, vol. 387, pp. 268–278, 2020. 3
- [69] Y. Wang, Z. Wang, Y. Lin, L. Khan, and D. Li, "Cifdm: continual and interactive feature distillation for multi-label stream learning," in *Proceedings of the 44th International ACM SIGIR Conference on Research and Development in Information Retrieval*, 2021, pp. 2121–2125. 3
- [70] J. Thadajarassiri, T. Hartvigsen, W. Gerych, X. Kong, and E. Rundensteiner, "Knowledge amalgamation for multi-label classification via label dependency transfer," in *Proceedings of the AAAI Conference on Artificial Intelligence*, vol. 37, no. 8, 2023, pp. 9980–9988. 3
- [71] H. Touvron, M. Cord, A. Sablayrolles, G. Synnaeve, and H. Jégou, "Going deeper with image transformers," in *ICCV*, 2021, pp. 32–42. 5
- [72] X. Tao, X. Hong, X. Chang, S. Dong, X. Wei, and Y. Gong, "Few-shot class-incremental learning," in *CVPR*, 2020, pp. 12 183–12 192. 6
- [73] H. Cha, J. Lee, and J. Shin, "Co2l: Contrastive continual learning," in *ICCV*, 2021, pp. 9516–9525. 6
- [74] T.-Y. Lin, M. Maire, S. Belongie, J. Hays, P. Perona, D. Ramanan, P. Dollár, and C. L. Zitnick, "Microsoft coco: Common objects in context," in *ECCV*. Springer, 2014, pp. 740–755. 7
- [75] M. Everingham, L. Van Gool, C. K. Williams, J. Winn, and A. Zisserman, "The pascal visual object classes (voc) challenge," *International Journal of Computer Vision*, vol. 88, no. 2, pp. 303–338, 2010. 7
- [76] F. Zhu, X.-Y. Zhang, C. Wang, F. Yin, and C.-L. Liu, "Prototype augmentation and self-supervision for incremental learning," in *CVPR*, 2021, pp. 5871–5880. 10